The Reaction of Nitrogen Dioxide with Sea Salt Aerosol

David D. Weis[†] and George E. Ewing*

Department of Chemistry, Indiana University, Bloomington, Indiana 47405

Received: November 19, 1998; In Final Form: April 15, 1999

The reaction of sea salt aerosol with NO_2 under ambient conditions was explored using particles that were generated by atomizing an aqueous solution of synthetic sea salt. The aerosol at 9−30% relative humidity, was mixed with 1−3 mbar of NO_2 and then passed through an optical cell where reactants and products were monitored by infrared spectroscopy. The duration times of the reaction, partial pressure of NO_2, and relative humidity were systematically varied in order to explore the aerosol heterogeneous chemistry. Infrared spectra of the aerosol revealed that a substantial fraction of the particulate Cl^- was replaced by NO_3^- and that there was a significant production of ClNO, consistent with the stoichiometery $2\ NO_2 + Cl^- \rightarrow NO_3^- + ClNO$. The rate of the reaction was found to increase both with NO_2 pressure and relative humidity. The infrared spectra also revealed that, even under arid conditions, the sea salt aerosol particles contain more water than can be explained by the various hydrates in sea salt, suggesting that the particles possess a complex structure. This complex structure involves microcrystalline and amorphous regions with pockets for water inclusions.

Introduction

It is estimated that sea salt is the largest source of tropospheric aerosol particulate matter with 10^{12} kg introduced into the atmosphere from wave action over the oceans each year.[1] Recently, considerable attention has been given to heterogeneous reactions between salts and nitrogen oxides and their possible roles in atmospheric chemistry, primarily as potential sources of tropospheric halogens. Chloride salts are known to participate in a variety of heterogeneous chemical reactions such as A,[2−11] B,[7,12−19] C,[20,21] and D:[13,22−24]

$$2NO_2(g) + Cl^-(p) \rightarrow NO_3^-(p) + ClNO(g) \qquad (A)$$

$$HNO_3(g) + Cl^-(p) \rightarrow NO_3^-(p) + HCl(g) \qquad (B)$$

$$ClONO_2(g) + Cl^-(p) \rightarrow NO_3^-(p) + Cl_2(g) \qquad (C)$$

$$N_2O_5(g) + Cl^-(p) \rightarrow NO_3^-(p) + ClNO_2(g) \qquad (D)$$

As usual (g) refers to the gas phase. The symbol (p) implies that Cl^- might be in aqueous solution or incorporated in a solid, but it is in some way associated with a condensed phase particle. Reactions A, C, and D are of particular interest because of their potential to form tropospheric chlorine radicals through the photolysis of ClNO, $ClNO_2$, and Cl_2. (The HCl formed in reaction B is highly soluble in H_2O and thus is rapidly lost from the gas phase.) The chlorine radicals are powerful oxidants in the troposphere and can facilitate ozone formation by a series of reactions with trace atmospheric components.[25,26]

Recent work by Finlayson-Pitts and co-workers with synthetic sea salt has shown that the presence of stable hydrates in sea salt can significantly alter the chemistry of reactions A and B.[11,17] Despite the differences between neat NaCl and sea salt, only a few studies have substituted sea salt for NaCl.[8,11,17] As shown elsewhere,[27,28] NaCl aerosol particles even at low humidity can contain significant amounts of included liquid water, in a form that may not be reproduced in the bulk material. The majority of the studies of reactions A−D have used supported solids (powders or large crystals) as the substrate.[3−7,9−17,19−22,24] Only a few aerosol chamber studies of these reactions have been reported,[2,8,18] and each was limited because the particles were analyzed by collection on filters followed by chemical analysis and thus were not in situ aerosol experiments. Furthermore, only one of these studies permitted the detection of gas-phase reactants and products.[18] To date there appear to be no direct in situ spectroscopic measurements of any of these reactions in an aerosol system. Here we report such a study, in this case the reaction of NO_2 with sea salt aerosol, at low humidity (less than 30%, RH = relative humidity) that is monitored by Fourier transform infrared (FT-IR) spectroscopy. Both gaseous and condensed phase reactants and products were detected in situ and in real time. It will be shown that under the conditions of the experiment, the reaction proceeds quite readily with a large yield of NO_3^-.

Experimental Section

Sea salt aerosols were generated from a solution of synthetic sea salt (Instant Ocean, Aquarium Systems, Inc.) in water (Alfa Aesar ultrapure spectrophotometric grade). The chemical composition of Instant Ocean is given in Table 1. Instant Ocean (hereafter referred to simply as sea salt) is carefully formulated to match the composition of natural sea salt and is specified to be nitrate free. Sea salt in water with a concentration of 0.1 kg of anhydrous solute per dm^3 of solution was prepared. After mixing the sea salt with water it was necessary to filter out a small amount (∼0.1% of the total solute mass) of precipitate that formed. Sodium nitrate aerosols were generated from a solution of $NaNO_3$ (Aldrich, reagent grade) dissolved in ultrapure water with a total solute concentration of 0.2 kg per dm^3 of solution.

[†] Present address: Department of Chemistry and Biochemistry, Middlebury College, Middlebury VT 05753. E-mail: dweis@middlebury.edu.

* To whom correspondence should be addressed.

10.1021/jp984488q CCC: $18.00
Published on Web 06/09/1999

TABLE 1: Chemical Composition[a] of Instant Ocean[61]

component	mole %	mole % (anhydrous)
Cl^-	38.10	48.80
Na^+	32.53	41.66
Mg^{2+}	3.78	4.84
SO_4^{2-}	1.96	2.50
K^+	0.77	0.95
Ca^{2+}	0.72	0.92
HCO_3^-	0.23	0.29
B	0.04	0.05
H_2O	21.92	0.00

[a] Accounts for 99.99% of the mass of Instant Ocean.

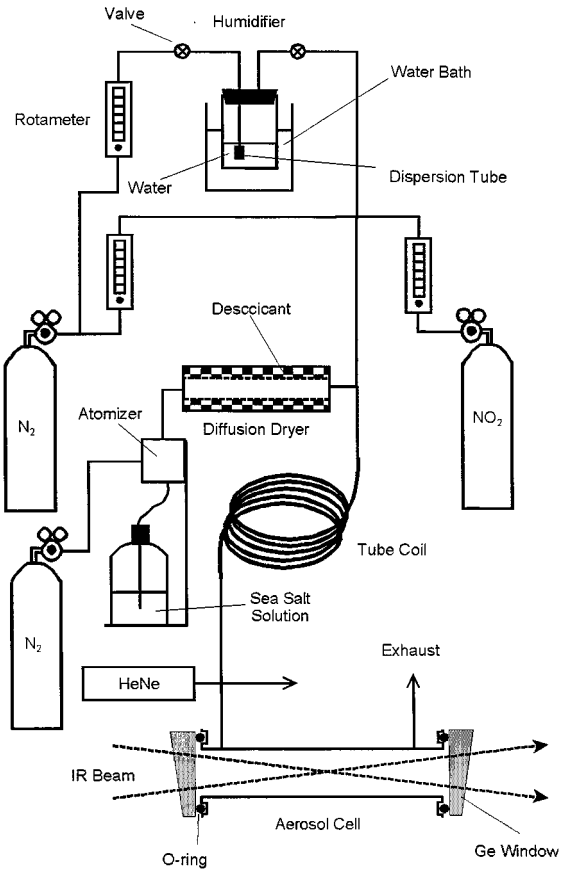

Figure 1. Schematic diagram of the experimental apparatus. See text for details.

A schematic of the experimental apparatus is shown in Figure 1. All of the tubing that was exposed to the reactant gas mixture was made of a fluoroethylene polymer (Nalgene 890), and all fittings were either stainless steel or fluoroethylene polymer. The solutions were atomized into submicron droplets using a constant output atomizer (model 3076, TSI, Inc.) driven by 2.5 bar of N_2 (UHP/zero grade, Air Products). The manufacturer specifies that the atomizer produces a log-normal distribution of droplets diameters[29] with a median diameter, $\bar{d}$, of 0.35 μm, a geometric standard deviation, ζ, of 2, and a number density, D_{part}, of 10^{14} particles m^{-3} of aerosol volume. After generation, the aerosol passed through a diffusion dryer (model 3062, TSI, Inc.) that consisted of a tube of wire cloth surrounded by silica gel desiccant. As the aerosol passed through the tube, water vapor was adsorbed onto the silica gel reducing the humidity to ~30% RH.

After passing through the dryer, the $NaNO_3$ aerosol was mixed with N_2 to achieve 13 ± 2% RH. The sea salt aerosol was mixed with a stream of N_2, NO_2, and in some experiments, H_2O vapor. Water vapor was added by bubbling N_2 through two coarse gas dispersion tubes (Ace Glassware) immersed in liquid water. The entire bubbler assembly was held at about 5 °C above ambient temperature with a stirred temperature-controlled water bath. The ratio of humid-to-dry N_2 was controlled by adjusting the relative flow rates through two rotameters. The total flow rate of the two gas streams was maintained at $(7 \pm 1) \times 10^{-2}$ dm^3 s^{-1}. Nitrogen dioxide was added to the stream from a compressed mixture of 1% NO_2/99% N_2 (BOC Gases). The flow rate of the NO_2/N_2 mixture (up to 0.03 dm^3 s^{-1}) was controlled with a precision nitrogen-calibrated rotameter (Omega). All gases were introduced at approximately 1.2 bar and thus with a slight overpressure. The resulting partial pressure of NO_2, calculated from the dilution factors, could be varied between 1 and 3 mbar. The aerosol was mixed with the gas stream and the combined flow was directed through the infrared (IR) optical cell.

In some experiments, a coiled fluoroethylene tube with an inner diameter of 1.1 cm and a length from 5 to 13 m was inserted between the point at which the gases mix with the aerosol and the IR cell. Changing the length of the tube varied the residence time of the aerosol particles, and thus the time of exposure to NO_2, from 3 to 13 s. The residence time was determined by measuring the time lag between the beginning of atomization and the arrival of the first particles in the cell. The arrival was determined by the observation of scattered light from a helium neon laser beam directed through the transparent tubing just upstream from the aerosol cell. The presence of the particles as indicated by the scattering of the laser light was easy to observe by eye. The uncertainty in the time measurement was approximately ±1 s. During the course of an experimental run, there was some visible accumulation of salt on the walls of the tubing.

The IR cell was made of Pyrex and had an optical path length of 12 cm and an inside diameter of 2.5 cm. The ends were sealed with germanium windows having a 30 min wedge (Infrared Optical) to eliminate etalon fringes and held in place with O-rings and clamps. The windows were oriented as shown in Figure 1. The cell was positioned in the sample compartment of the FT-IR spectrometer such that the focus point of the IR beam was near the center of the cell.

Spectra were obtained with a Nicolet Magna 550 FT-IR equipped with a mercury−cadmium−telluride (MCT) detector. The interferograms were recorded at 4 cm^{-1} resolution without zero filling and were triangle apodized prior to being fast Fourier transformed to obtain single beam spectra. Extinction spectra $E(\tilde{\nu})$ were obtained from

$$E(\tilde{\nu}) = \log_{10}\left(\frac{I_0(\tilde{\nu})}{I(\tilde{\nu})}\right) \quad (1)$$

where $I_0(\tilde{\nu})$ is the background single beam spectrum of the N_2-purged cell and $I(\tilde{\nu})$ is the single beam spectrum of the cell containing aerosol. The background single beams were obtained by averaging 200 interferograms, while the aerosol single beams were the average of 100 interferograms.

The percent relative humidity (% RH) of the aerosol was determined spectroscopically by measuring the integrated extinction by H_2O vapor from 2000 to 1250 cm^{-1}. The percent relative humidity is given by

$$\%\ \mathrm{RH} = \frac{P_{H_2O}}{P^\circ_{H_2O}} 100\% \quad (2)$$

where $P^\circ_{H_2O}$ is the equilibrium vapor pressure of H_2O. A

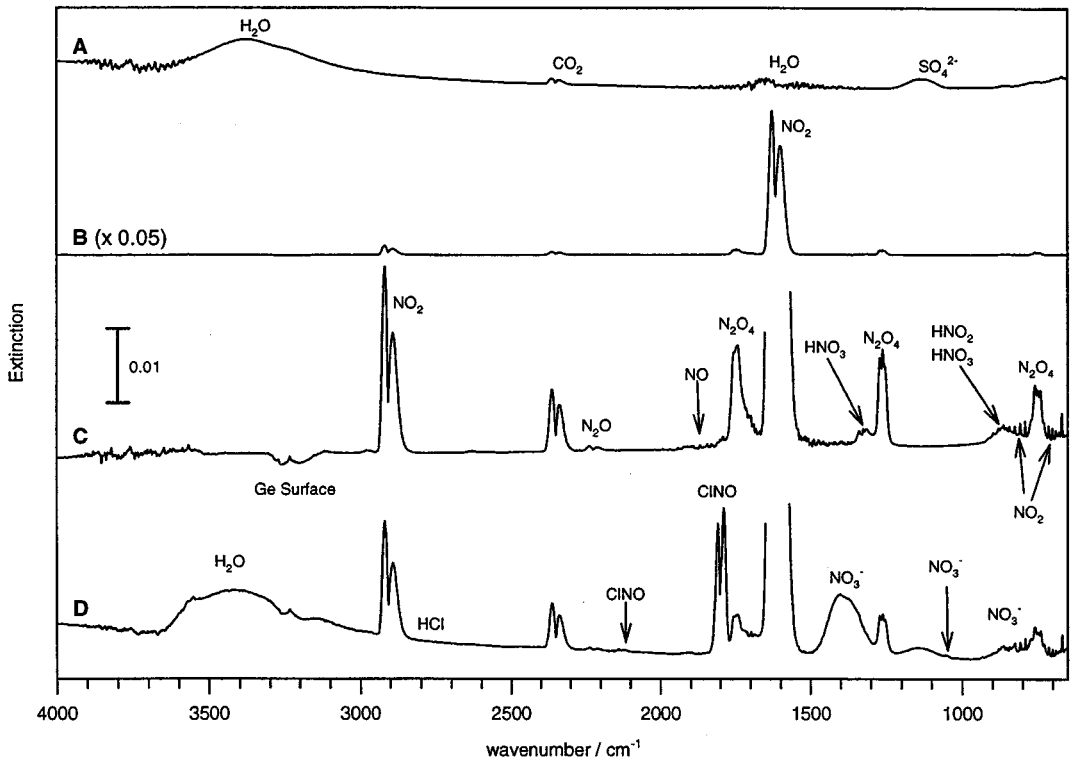

Figure 2. Survey spectra at 27 ± 4% RH. Spectrum A, Sea salt aerosol; spectra B and C, NO_2 with H_2O; spectrum D, sea salt aerosol exposed to 3 mbar NO_2 with H_2O for 7 s. The prominent absorption bands in the spectra have been assigned. See the text and Table 2 for the details of the assignments.

calibration curve of integrated extinction versus relative humidity was constructed by measuring the relative humidity of the gas stream in the absence of aerosol with a digital hygrometer (Hanna Instruments HI8564). All measurements were taken at a total pressure of 1.2 ± 0.1 bar (consisting mostly of N_2) and a temperature of 23 ± 2 °C. Because of the ±2 °C uncertainty in the gas temperature, there was a ±15% uncertainty in $P^{\circ}_{H_2O}$.[30] This uncertainty introduces a systematic, rather than random error, into the humidity calculation.

In most of the spectra, H_2O vapor produced the dominant features, obscuring the 4000−3400 cm^{-1} and 2000−1400 cm^{-1} regions. The interfering water vapor absorption can be dramatically reduced (but not completely eliminated[31]) through the use of scaled absorbance subtraction of a spectrum of pure H_2O vapor. The FT-IR software permits this subtraction to be done interactively by allowing the user to manually scale the subtraction factor until the H_2O absorption is minimized.

In a typical experimental run the reactant gas mixture was allowed to flow through the cell for between 2 and 5 min prior to the introduction of aerosol. Aerosol was then added to the gas mixture, and its residence time was measured. After 1−2 min of atomization, two consecutive spectra were taken, each requiring approximately 1 min of acquisition time. Following the collection of spectra, the cell was flushed with N_2.

Results

Figure 2 shows survey spectra of a sea salt aerosol in spectrum A, a mixture of NO_2 and H_2O in spectra B and C, and a sea salt aerosol exposed to NO_2 and H_2O vapor in spectrum D, all at 27 ± 4% RH. Also shown in Figure 2 are assignments of the prominent features in the spectra. The absorption frequencies of band centers and the assignments are summarized in Table 2. The justifications for these assignments will be presented later. In addition to the various absorption bands in Figure 2, a rise in the base line toward higher wavenumbers is evident in the aerosol spectra A and D. This a consequence of scattering of light by the aerosol particles.[32,33]

The prominent features in the sea salt aerosol in spectrum A are the broad absorption bands due to liquid-phase H_2O and SO_4^{2-} as well as sharp features of atmospheric CO_2 and H_2O. The prominent features for NO_2 and H_2O in spectra B and C are assigned to the variety of nitrogen oxides (NO_2, N_2O, N_2O_4, NO) and associated acids (HNO_2, HNO_3) as well as a surface feature of the germanium windows. (Spectrum B reproduces spectrum C on a smaller scale.) Spectrum D of the sea salt reaction with NO_2 is in part a combination of the two previous spectra. In addition several new features are observed. Absorption bands of gas-phase ClNO are present as is NO_3^- within the particles. Absorption due to gas-phase HCl is also present, although with the scale of Figure 2 it is not apparent.

Figure 3 presents the 1500−1000 cm^{-1} region of the spectrum for sea salt aerosol before NO_2 exposure (0 s) and after exposure to 3 mbar NO_2 at 27 ± 4% RH for 7 and 11 s. Absorption features due to NO_3^-, N_2O_4, and SO_4^{2-} are assigned. The absorption by the NO_3^- band at 1400 cm^{-1} increases dramatically with exposure time. During this same time interval, absorption by N_2O_4 remains constant and the SO_4^{2-} feature decreases by ∼50%. A second NO_3^- band at 1055 cm^{-1} appears over this time interval.

Figure 4 shows the IR absorption in the 1500−1300 cm^{-1} region for a variety of nitrate-containing materials. The top spectrum, A, shows absorption by $NaNO_3$ produced by the reaction of NO_2 with the (100) faces of single-crystal NaCl.[10] Spectrum B is the absorption by single-crystal $NaNO_3$ derived[34] from imaginary index of refraction data of the bulk material.[35] Absorption by a thin film (∼1.6 μm) of 0.6 M aqueous $NaNO_3$ solution is shown in spectrum C.[36] Spectrum D is the extinction spectrum of $NaNO_3$ aerosol at 13 ± 2% RH described

TABLE 2: Assignments of Spectral Features

molecule	$\tilde{\nu}$/cm^{-1}	assignment	ref[a]
H_2O	3400	ν_1, ν_3	H
Ge surface	3258		
	3201		
HCl	2830−2700	ν_1	IUPAC
NO_2	2918	$\nu_3 + \nu_1$	AN, KN
	2891		
CO_2	2362	ν_3	H
	2337		
N_2O	2237	ν_3	MH
	2211		
ClNO	2139	$\nu_3 + \nu_1$	BB, LF
	2132		
	2119		
NO	1903	ν_1	M2,MH
	1875		
	1850		
ClNO	1808	ν_1	H, BB, LF
	1789		
N_2O_4	1754	ν_3	BE, MH
	1744		
H_2O	1650	ν_3	H
NO_2	1628	ν_1	AN, KN
	1600		
NO_3^-	1400	ν_3	H, KR
HNO_3	1339	ν_3	M1, MH
	1331		
HNO_3	1324	ν_4	M1, MH
	1314		
N_2O_4	1270	ν_{11}	BE, MH
	1261		
	1256		
SO_4^{2-}	1150	ν_3	H
NO_3^-	1050	ν_1	H, KR
NO_2	900−660	ν_2	AN, KN
HNO_3	879	ν_5	M1, MH
	869		
cis-HNO_2	868	ν_4	M2, MH
	853		
	842		
NO_3^-	841	ν_2	H, KR
trans-HNO_2	806	ν_4	M2, MH
	791		
	777		
N_2O_4	760	ν_{12}	BE, MH

[a] AN, Arakawa and Nielsen;[62] BB, Burns and Bernstein;[63] BE, Bibart and Ewing;[64] KN, Keller and Nielsen;[65] KR, Kato and Rolfe;[51] H, Herzberg;[43] IUPAC;[66] LF, Landau and Fletcher;[67] M1, McGraw et al.;[68] M2, McGraw et al.;[69] and MH, Mélen and Herman.[47]

previously. Spectrum E is the calculated extinction of crystalline $NaNO_3$ aerosol particles with $\bar{d} = 0.15$ μm and $\zeta = 2$ (the approximate size distribution of the $NaNO_3$ particles if dried completely). The calculation was performed using the program MIECALC,[37] which applies the BHMIE Mie theory program[34] to a log-normal distribution,[29] and the complex index of refraction of $NaNO_3$.[35] The spectrum labeled F, extracted from Figure 3, shows the extinction by a sea salt aerosol at 27 ± 4% RH after an 11 s exposure to 3 mbar of NO_2. (The asterisk denotes an overlapping absorption by HNO_3).

There are notable differences among the spectra shown in Figure 4. For spectrum A, the spectrum of $NaNO_3$ on the single-crystal NaCl faces, the absorption takes the form of a distinct doublet at 1416 and 1356 cm^{-1} with an approximately 1:3 absorbance ratio. The absorption spectrum of single-crystal $NaNO_3$ of spectrum B bears a strong resemblance to spectrum A, except that the high-frequency component overlaps with or is not resolved from the prominent low-frequency component. Although absorption by aqueous $NaNO_3$ in spectrum C is in the same spectral region as the absorption bands of solid $NaNO_3$,

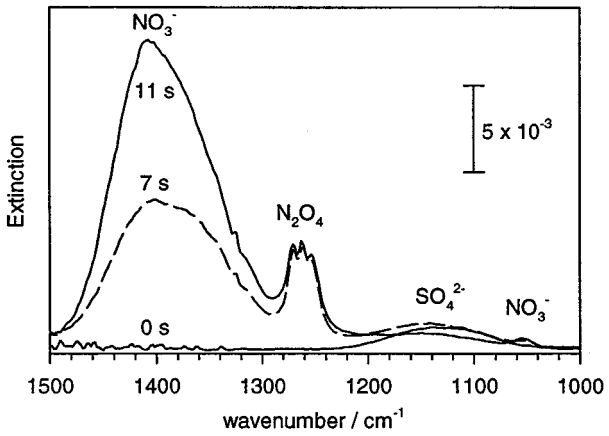

Figure 3. Temporal changes of sea salt aerosol spectra. The spectrum labeled 0 s is for the aerosol before NO_2 exposure. Spectra labeled 7 and 11 s are for the aerosol after exposure to 3 mbar NO_2. All aerosols were at 27 ± 4% RH.

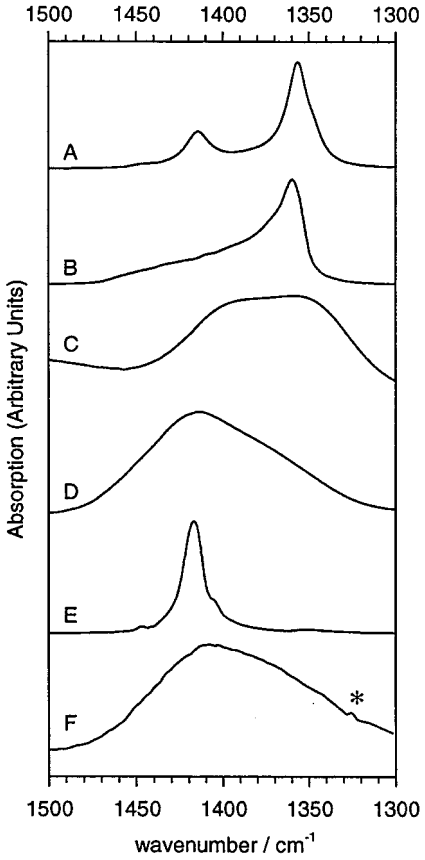

Figure 4. Infrared spectra of the nitrate region. The spectra are A, absorption from the reaction of NO_2 with single-crystal NaCl(100) faces;[10] B, the absorption spectrum of crystalline $NaNO_3$ derived from the imaginary index of refraction;[35] C; aqueous 0.6 M $NaNO_3$;[36] D, $NaNO_3$ aerosol at 13 ± 2% RH; E, the calculated spectrum for crystalline $NaNO_3$ aerosol; and F, sea salt aerosol after exposure to 3 mbar of NO_2 at 27 ± 4% RH, taken from Figure 2, spectrum D, where the asterisk denotes an overlapping absorption by HNO_3.

the shape of the band is distinct. The band is much broader, with a half-width of approximately 90 cm^{-1}, and is composed to two overlapping features at 1400 and 1350 cm^{-1} that, perhaps coincidentally, correspond with the absorption bands of spectrum A. The $NaNO_3$ aerosol spectrum in spectrum D centered at 1415 cm^{-1} of half-width 80 cm^{-1} is slightly asymmetric. The calculated $NaNO_3$ aerosol extinction spectrum in spectrum E consists of a prominent feature centered at 1415 cm^{-1}, a shoulder

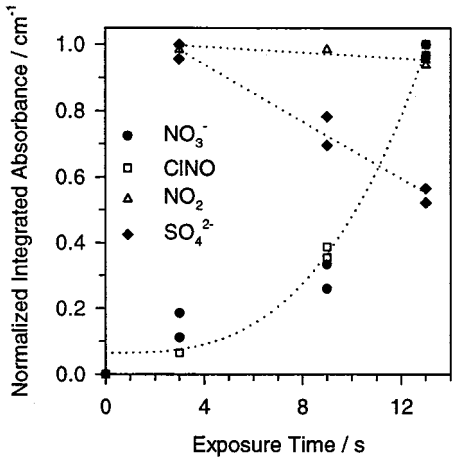

Figure 5. Normalized integrated absorbances for a sea salt aerosol at 9 ± 1% RH exposed to 2 mbar NO_2. The absorbances monitored were the NO_3^- band centered at 1400 cm^{-1}, ClNO at 2130 cm^{-1}, NO_2 at 2905 cm^{-1}, and SO_4^{2-} at 1150 cm^{-1}. The integrated extinction values were normalized independently so that the maximum value for each is 1. The dotted lines are guides for the eye.

at 1400 cm^{-1}, and a weak absorption at 1445 cm^{-1}. The spectrum of sea salt aerosol that has been exposed to NO_2, in spectrum F, contains a broad asymmetrical absorption band, of half-width 80 cm^{-1} centered at 1410 cm^{-1} that most closely resembles the $NaNO_3$ aerosol spectrum in spectrum D.

Figure 5 is a plot of the normalized integrated absorbance of the NO_2, ClNO, NO_3^-, and SO_4^{2-} versus exposure time for a sea salt aerosol with 2 mbar of NO_2 at 9 ± 1% RH. The integrated absorbance $\tilde{A}$, when the scattering contribution is negligible or has been removed, is given by

$$\tilde{A} = \int_{\text{band}} E(\tilde{\nu}) d\tilde{\nu} \qquad (3)$$

The integrated absorbance for each band was independently normalized so that the maximum value for each trace is 1. (If each trace was multiplied by an appropriate constant, the vertical axis would represent the concentration in molecules per unit volume.) Both ClNO and NO_3^- increase as the exposure time increases and the quantities track each other well. Sulfate decreases by about 50% and NO_2 decreases by about 5% over the same time interval. Similar trends were observed in all of the experimental runs.

Figure 6 shows the H_2O:salt molar ratio (the ratio of moles of condensed phase water to the total number of moles of ions in the salt aerosol particles) as a function of NO_2 exposure time. (The calculation of this molar ratio is discussed later.) For sea salt aerosol at 9 ± 1% RH (the open circles), there is little variation in this ratio as exposure time increases, with a mean value and standard deviation of 0.42 ± 0.03. However this ratio for bulk hydrated sea salt (calculated from the assay in Table 1) at 0.28 is considerably lower, indicating a significant water inclusion by the sea salt aerosol particles. Likewise water inclusion by $NaNO_3$ aerosol particles to a H_2O:salt ratio of 0.5 is observed. The time independent ratios for hydrated sea salt and $NaNO_3$ aerosol particles are indicated by the dashed lines in Figure 6. For sea salt at 27 ± 4% RH exposed to 2 or 3 mbar of NO_2 (the filled symbols), a temporal change in the H_2O:salt ratio is observed when nitrogen oxide chemistry is initiated. (The scatter in the 1 mbar data obscures any apparent trend.) At both NO_2 pressures, the ratio increases with exposure time. Furthermore, the H_2O:salt ratio also increases with increasing NO_2 pressure, from ~0.6 up to ~1.2, with the minimum ratio

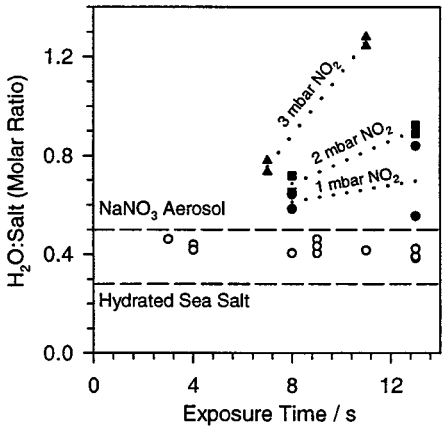

Figure 6. Molar ratio of water to sea salt as a function of NO_2 exposure time. The open symbols are for sea salt aerosol at 9 ± 1% RH exposed to 1, 2, and 3 mbar NO_2. The filled symbols are for sea salt aerosol exposure to (●) 1 mbar, (■) 2 mbar, and (▲) 3 mbar NO_2 at 27 ± 4% RH. The dotted lines are guides for the eye. The dashed horizontal lines give the molar ratios for the $NaNO_3$ aerosol at 13 ± 2% RH and bulk sample of hydrated sea salt.

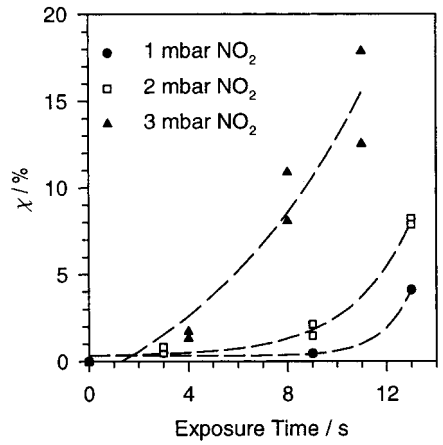

Figure 7. Conversion, χ, of sea salt aerosol at 9 ± 1% RH to NO_3^- as a function of exposure time to 1, 2, or 3 mbar of NO_2. The dashed lines are guides to the eye.

observed for a sea salt aerosol exposed to 1 mbar of NO_2 for 8 s and a maximum for sea salt aerosol exposed to 3 mbar of NO_2 for 11 s. In all cases the H_2O:salt ratio is higher at 27 ± 4% RH than at 9 ± 1% RH.

Figures 7 and 8 show the extent of conversion, χ (expressed as a percent), of Cl^- to NO_3^-, as a function of exposure time. Figure 7 shows results at 9 ± 1% RH, and Figure 8 shows results for 27 ± 4% RH. The quantitation to obtain χ is presented below. In both figures, χ increases markedly with both increasing exposure time and with increasing NO_2 pressure. The maximum values of χ after 11 s of exposure to 3 mbar of NO_2 were 15% for sea salt aerosol at 9 ± 1% RH and 80% for sea salt aerosol at 27 ± 4% RH.

Discussion

1. Assignment of Spectral Features. The spectra shown in Figure 2 are rich with absorption features. Table 2 contains their assignments. We begin with a discussion of the sea salt aerosol spectrum A of Figure 2. The broad absorption features at 3400 and 1650 cm^{-1} are signatures for the presence of liquid-phase H_2O.[38−42] Similar absorption features have been observed by us[27] and by Cziczo et al.[28] in IR spectra of (water-containing) NaCl aerosols. Later, we shall use the H_2O absorption band at

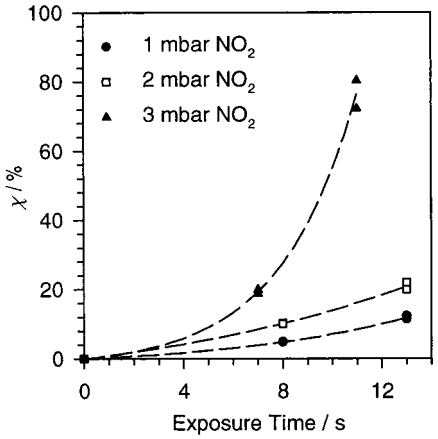

Figure 8. Conversion, χ, of sea salt aerosol at 27 ± 4% RH to NO_3^- as a function of NO_2 exposure time. The dashed lines are guides to the eye.

3400 cm^{-1} to determine the water content of the sea salt aerosol particles. Atmospheric CO_2, with its characteristic absorption at 2350 cm^{-1}, appears in the spectra because of instabilities in the spectrometer purge and from its presence in the liquid water components of our experimental apparatus. Absorption by SO_4^{2-} is evident at 1100 cm^{-1}, consistent with other studies.[28,32,33,43−45] However, in contrast to the narrow SO_4^{2-} absorption band in crystalline $(NH_4)_2SO_4$,[28,32,33,44,45] its absorption in sea salt is diffuse. Later we shall use SO_4^{2-} as an internal standard to determine the mass of sea salt in the aerosol particles.

Now we turn to the IR spectrum of the reactant gases at 27 ± 4% RH in spectra B and C of Figure 2. The negative-going doublet centered near 3230 cm^{-1} appears whenever NO_2 is introduced into the cell and disappears when the NO_2 is flushed out. This indicates that there is some background absorption that is diminished in the presence of NO_2. Germanium is known to react spontaneously with concentrated nitric acid.[46] Thus there may be a reversible loss of a surface species from the Ge windows when they are exposed to NO_2 or HNO_3 vapor. The frequency region of the feature is consistent with hydride or hydroxide vibrations that might be expected to exist on the Ge surface until removed by nitrate formation. When the reactive gases are removed from the cell, the surface-bound species returns. The absorption bands of the various gas-phase nitrogen oxides are well-known,[47] and their assignments have been made on the basis of the references given in Table 2. Although spectra B and C were obtained at 27 ± 4% RH, spectra of the arid (≪1% RH) 1% NO_2/ 99% N_2 reactant gas mixture revealed these same absorption features of trace nitrogen oxides but in lower proportions. The presence of NO, N_2O, HNO_3, and HNO_2 can be expected in any mixture containing both H_2O and NO_2 (or any other nitrogen oxides for that matter),[47] making the mixture considerably more complicated and necessitating the consideration of reactions involving nitrogen oxides other than NO_2. (These reactions will be considered in section 4.)

Now we turn our attention to the spectrum of sea salt aerosol exposed to NO_2 (and its accompanying trace nitrogen oxides) that is shown in spectra D of Figure 2. In addition to the absorption features observed in the previous spectra, several new bands are present. The presence of HCl vapor is confirmed by the observation of the portion of its vibrational−rotational structure not obscured by stronger absorption by other species (results not shown). Absorption bands assigned to NO_3^- modes are found at 1400, 1050, and 841 cm^{-1} as identified in spectrum D of Figure 2 and listed in Table 2. In addition Figure 4 presents a detail of the 1400 cm^{-1} region for NO_3^- in a variety of environments. We will explore the implications of these differences in section 3.

To summarize, then, both of the principal reactants (NO_2 and Cl^-) and both of the principal products (NO_3^- and ClNO) have been measured through IR spectroscopy in the aerosol system. NO_2, ClNO, and NO_3^- were all detected directly by their IR absorption bands. The reactant, Cl^- (as NaCl or other chlorides), was measured indirectly by the presence of SO_4^{2-} that is a known component of the sea salt. In addition, other gas-phase nitrogen oxides: NO, N_2O, N_2O_4, HNO_3, and HNO_2, are present in smaller amounts. Trace amounts of gas-phase HCl were also detected. While we use the adjective "trace" one could argue that a large amount of HCl was produced but was then adsorbed on the walls of the apparatus or dissolved in water associated with the aerosol particles making it hidden from our spectroscopic probe. We shall provide other evidence later that suggests that HCl is indeed not a principle product.

2. Quantitation. The concentration of molecules in the aerosol can be determined by using a modified Beer−Lambert relation,

$$D_x = \frac{2.303(10^2)\tilde{A}}{\bar{\sigma}_x z} \tag{4}$$

where D_X is number of X molecules per unit volume of the aerosol sample and $\bar{\sigma}_X$ is the integrated absorption cross section per molecule. The optical cell path length is z. (The factor 10^2 converts the integrated absorbance $\tilde{A}$, obtained in cm^{-1} units to SI units of m^{-1}.) The integrated absorption cross section may be obtained from the frequency dependent imaginary component of the index of refraction using relationships given elsewhere.[32,34] The values obtained are $\bar{\sigma}_{H_2O} = 1.3 \times 10^{-18}$ m molecule^{-1} in the OH stretching region for 5M NaCl solution,[48] $\bar{\sigma}_{SO_4^{2-}} = 2.5 \times 10^{-18}$ m molecule^{-1} from single crystal $(NH_4)_2SO_4$,[44] and $\bar{\sigma}_{NO_3^-} = 3.0 \times 10^{-18}$ m molecule^{-1} for the ν_3 mode of NO_3^- integrated over the 1500−1300 cm^{-1} region.[35]

Aside from broad low-frequency (∼300 cm^{-1}) phonon modes,[44] NaCl has negligible absorption in the infrared or visible regions and hence, cannot be detected directly by our spectroscopy. Nevertheless the chloride concentration D_{Cl^-} in sea salt aerosol can be determined if an appropriate IR active internal standard is present. Fortuitously, dry sea salt is 2.5 mole % SO_4^{2-} and the spectroscopy of sulfate-containing aerosols has already been well characterized.[32,33] The chloride concentration D_{Cl^-} can then be calculated directly from the ratio of Cl^- to SO_4^{2-} in sea salt (see Table 1):

$$D_{Cl^-} = \frac{49.1\%}{2.5\%} D_{SO_4^{2-}} \tag{5}$$

Similarly, any other component of sea salt can be calculated from the molar percentages listed in Table 1. In particular, D_{salt}, the total concentration of *anhydrous* solute per m^3 of cell volume is given by

$$D_{salt} = \frac{97.5\%}{2.5\%} D_{SO_4^{2-}} \tag{6}$$

Thus, it is possible to calculate the extent of conversion χ of Cl^- to NO_3^-:

$$\chi = \frac{D_{NO_3^-}}{D_{Cl^-}} \times 100\% \tag{7}$$

Although there was some accumulation of salt on the walls of the tubing during the course of these experiments, the determination of χ is not affected by this. While the gases in the system may react with sea salt that adheres to the walls of the system, this fraction of the reactions will not be observed since the resulting NO_3^- will remain attached to the walls and thus will not reach the IR cell. This does mean, however, that an analysis of the kinetics on the basis of the gases might require corrections because of wall reactions. In the next section, D_{salt} and D_{H_2O} and the structure of the NO_3^- absorption band will be used to evaluate the particle composition and morphology.

3. Composition and Morphology. Figure 6 shows that at 9 ± 1% RH the water:salt molar ratio (i.e., D_{H_2O}:D_{salt}) is 0.42 ± 0.03. Referring to Table 1, solid sea salt is 22 mole % H_2O giving a water:salt ratio of 0.28. (Nearly all of this water can be accounted for by the presence of $MgCl_2 \cdot 6H_2O$.[49]) Thus the water:salt ratio is 50% larger than would be predicted based on the hydrates present in solid sea salt. The ratio is consistent with a recent deliquescence/efflorescence investigation by Tang et al.[50] Treating sea salt as NaCl and estimating from Figure 1 of Tang et al.,[50] the water:salt ratio at 9% RH is 0.6 ± 0.2, in good agreement with our observations. What is more, Tang et al.[50] reported that even under vacuum, sea salt particles retain residual water. IR spectroscopic studies of submicron NaCl particles at low humidity (<25% RH) reveal that a significant amount of water is present in the form of small inclusions of liquid water.[27,28] Again estimating from the results of Tang et al.,[50] the water:salt ratio at 27% RH is 1.0 ± 0.3, consistent with our observations at 27 ± 4% RH. If the water:salt ratio did not show an NO_2 pressure dependence at 27 ± 4% RH, our results would suggest that the sea salt particles were not at equilibrium with water vapor at short exposure times. As it is, however, these results suggest that NO_3^- formation facilitates the uptake of H_2O by the particles or increases their capacity to incorporate H_2O. A similar increase in the water content of sea salt powders exposed to NO_2 in an atmosphere with less than 2 ppm of H_2O vapor has been observed in another infrared study.[11] The mechanism by which NO_3^- formation leads to increased water content at 27 ± 4% RH but not at 9 ± 1% RH is not clear.

It is perhaps surprising that the NO_3^- infrared signatures, as revealed by the six spectra of Figure 4, can be so different. To understand these differences, and how they concern the theme of our study, we need to explore the symmetry of the ion isolated and in various condensed phases. The isolated ion is planar and belongs to the D_{3h} point group.[43] It has five infrared active modes: the nondegenerate $\nu_2(a_2'')$ out-of-plane bending vibration at 831 cm^{-1}, $\nu_3(e')$ antisymmetric stretching vibrations at 1390 cm^{-1}, and $\nu_4(e')$ in-plane bending vibrations at 720 cm^{-1}, the latter two being doubly degenerate. An infrared inactive mode $\nu_1(a_1')$, the symmetric stretching vibration, is at 1050 cm^{-1}. In keeping with previous discussion of nitrate spectra produced by nitrogen oxides reacting with NaCl,[7,10] the spectroscopic labels are made as if the NO_3^- ion were isolated. Thus the features in spectrum C of Figure 2 are assigned: 1400 cm^{-1} to ν_3, 1050 cm^{-1} to ν_1 and 841 cm^{-1} to ν_2. The ν_4 absorption is roughly 2 orders of magnitude weaker than the ν_3 absorption,[51] and thus we were unable to detect it. Note that the observation of the ν_1 mode in both the $NaNO_3$ aerosol spectrum (not shown) and in spectrum D of Figure 2 indicates that the environment must lower the D_{3h} symmetry of NO_3^- to give this vibration infrared activity.

That environments can lower the local symmetry of NO_3^- has been made evident in spectroscopic investigations of the aqueous ion.[52,53] For example, infrared studies of dilute solutions of $NaNO_3$ by Irish and Davis[53] show a splitting of $\nu_3(e')$ into two overlapping features at 1405 and 1346 cm^{-1}. They assign these features to $\nu_4(b_1)$ and $\nu_1(a_1)$, respectively, with spectroscopic labels in accord with the C_{2v} point group they propose for the NO_3^- ion solvated by water in the solution. We have reproduced their results in our laboratory[36] as shown in spectrum C of Figure 4 where the diffuse doublet is apparent. The $\nu_4(b_1)-\nu_1(a_1)$ difference of approximately 60 cm^{-1} for a variety of salts, on extrapolation to infinite dilution, is consistent with the view that solvated NO_3^- is in an environment that is essentially independent of the cations. However, at higher concentrations, the $\nu_4(b_1)-\nu_1(a_1)$ difference depends on the nature of the cation.

Obviously nitrate ions are not isolated in solid $NaNO_3$ which forms rhombohedral crystals.[54] The unit cell contains two planar NO_3^- ions lying one above the other with their oxygen atoms staggered. (The 3-fold axis through the N atoms is the trigonal axis of the unit cell.) The point group symmetry of the two nitrate groups (like that of staggered CH_3CH_3) is D_{3d}. The antisymmetric stretching vibrations that characterize the isolated ions, of type $\nu_3(e')$, then couple for the two ions of the unit cell, to give (by analogy to the D_{3d} CH_3CH_3 normal mode discussion[43]) four vibrational modes. One, $\nu_7(e_u)$, is doubly degenerate and infrared active with transition dipoles directed orthogonal to the trigonal axis of the rhombohedral unit cell. The other, $\nu_{10}(e_g)$, is also doubly degenerate but infrared inactive. In spectrum B of Figure 4, the $\nu_7(e_u)$ mode is the prominent feature. Nevertheless, the resulting spectrum is the consequence of the coupling of transition dipoles of the unit cells that make up the (in principle) infinite crystal lattice. If on the other hand, the crystal is small as in the case of aerosol particles the extent of coupling is limited by the finite boundaries of the tiny crystals.[34] The spectroscopic result, a consequence of the Mie calculation, is shown in spectrum E of Figure 4. As in another salt we have examined, $(NH_3)_2SO_4$, the calculated band center of the aerosol particles is also shifted to higher frequency relative to the bulk crystal.[32] These spectroscopic differences are a consequence of molecular and ionic crystals made up of transition dipoles that couple together. The resultant spectra, as revealed in the changed band center of the $\nu_7(e_u)$ feature in spectra B and E, depend on the size of the crystal.[55,56] Although we have somewhat arbitrarily chosen $\bar{d} = 0.15$ μm and $\zeta = 2$ for this calculation, within the Rayleigh limit the structure of the extinction band is not size dependent.[32,34]

Spectroscopic differences can also result from changes in the shape of crystals.[55,56] A single feature that results from isotropic cubic or spherical crystals as in spectra B and E, respectively, can be split when the crystal appears as a thin plate or needle. This has been observed by Devlin et al.[57] who prepared a thin crystalline plates of $NaNO_3$ on the surface of a substrate. Since the crystal is no longer isotropic (i.e. it is not a cube but a thin plate), the $\nu_7(e_{2u})$ degeneracy is lifted. The resulting frequencies were found at 1450 and 1350 cm^{-1}. A possible interpretation of spectrum A of Figure 4 is that thin crystalline plate of $NaNO_3$ have been produced over the NaCl(100) substrate by reaction of nitrogen oxides with it. Alternatively, as Peters and Ewing suggest,[10] the NO_3^- ion finds itself imbedded in a site of the NaCl substrate that lowers the D_{3h} symmetry of the isolated ion to lift the $\nu_3(e')$ degeneracy.

A pattern so far apparent in the spectroscopic signatures of Figure 4 is that spectra A, B, and E, which are characterized by sharp features, are associated with NO_3^- ions in crystalline environments. The spectra in spectra C, D, and F are all more

diffuse. Since we know that the sample giving rise to spectrum C is amorphous (actually liquid), it is reasonable to suggest that the samples associated with spectra D and F are also amorphous. Moreover, the similarities in band center, bandwidth, and band shape of their spectra suggest a similarities in the environments of the NO_3^- ions in these aerosol samples. Finally, we note that the frequencies of the band centers of spectra D and F most closely match the band center of the neat $NaNO_3$ crystalline aerosol calculation of spectrum E. Therefore, on the basis of the spectroscopic signatures alone, we would say that spectra D and F are consistent with what we would expect for an aerosol of amorphous NO_3^-.

Fung and Tang[58] have obtained Raman spectra of the ν_1 mode of NO_3^- in $NaNO_3$ and $Sr(NO_3)_2$ single levitated particles. In both cases, the band is broad and structureless for the aqueous droplet. Upon efflorescence of the $NaNO_3$ particle, the band sharpens considerably, with the bandwidth decreasing by roughly a factor of 5, and shifts to higher frequency. As the humidity is lowered, the $Sr(NO_3)_2$ droplet did not effloresce, instead it retained a significant amount of water for a 1:1 water:solute molar ratio. Again, the Raman band of crystalline $Sr(NO_3)_2$ is sharper, structured, and at higher frequency than the band of the hydrous particle. Thus, the spectroscopic signature on the ν_1 mode of NO_3^- is altered as the water composition and phase of the particle change.

The behavior of the ν_3 mode of NO_3^- in this study is likewise sensitive to the association of water with the particle. In Figure 4, the extinction spectrum of $NaNO_3$ calculated from the index of refraction for crystalline $NaNO_3$ is a (relatively) narrow band with some structure. The extinction bands of the $NaNO_3$ aerosol and of the sea salt aerosol exposed to NO_2 are considerably broader and featureless. In both of these cases, the water:salt ratio is quite high (approximately 0.5 and 1.2, respectively). We conclude then that sea salt particles, even at low humidity, have a complex morphology.

The structure of the sea salt particles may be further complicated because the various salts in sea salt probably do not effloresce into a uniform solid but rather form individual domains of varying composition. Cheng et al.[59,60] placed ~100 μm droplets of seawater on a silicone-coated glass slide (with a contact angle of 90°) and allowed the droplets to evaporate. They observed a sequential formation of microcrystals that corresponded to the concentration and solubility of the various salts present in seawater. Furthermore, the microcrystals had different sizes and structures that depended on their composition. In addition to the changing spectroscopic signatures of the NO_3^- ion with its condensed phase environment, we can also follow the response of the ν_3 mode of SO_4^{2-}. In the aerosol prepared with water solutions of neat $(NH_4)_2SO_4$, the ν_3 half-width is 40 cm^{-1},[32] whereas in the sea salt aerosol (see Figure 3) its half-width is twice as great. Thus we imagine the sea salt particles to be internal mixtures of microcrystalline and amorphous regions of varying composition and shape with inclusions of aqueous salt solution.

4. Reaction Mechanism and Kinetics. The variety of nitrogen oxide species evidenced in Figure 2 requires us to consider the possibility that reactions such as reaction B may be competing with reaction A. The nitric acid reaction with sea salt is of particular concern because the reaction probability for reaction B is roughly 7 orders of magnitude larger than the reaction probability of reaction A.[11,17] However, with the exceptions of NO_2 and N_2O_4, all of the remaining nitrogen oxides (NO, N_2O, HNO_2, and HNO_3) are present only in trace amounts and thus cannot contribute to the observed formation of NO_3^-. In addition, the prominence of the ClNO product of reaction A and its favorable tracking of its integrated absorbance with that of NO_3^- (Figure 5) favors reaction A as the dominant reaction.

There remains the issue of whether the reactive molecule is NO_2 or its dimer, N_2O_4. Although many kinetic studies clearly show that the reaction is second order with respect to NO_2,[4,7,10,11] consistent with N_2O_4 as the reactive species, there is no direct evidence that N_2O_4 is the reactive molecule. Second-order kinetics would also be consistent with, for example, adsorption of two separate NO_2 molecules at adjacent sites on the substrate followed by an oxygen atom transfer. For this reason, we prefer to express reaction A as written, with the understanding that the equation indicates only the stoichiometry of the reaction.

Given the complexity of the reactants (both the sea salt and the nitrogen oxides), the high and variable water content of the particles, and the limited number of data points, it is not surprising that straightforward kinetics do not emerge. Nevertheless, some recent findings in similar reaction systems may be brought to bear here. Langer et al.[11] studied the reaction of NO_2 with solid sea salt and with $MgCl_2 \cdot 6H_2O$ (as a surrogate for all hydrates in sea salt) using diffuse reflectance Fourier transform IR spectroscopy (DRIFTS). They found that the IR spectra of the product NO_3^- from the reaction of NO_2 with sea salt was the same as that from the reaction of $MgCl_2 \cdot 6H_2O$ with NO_2, thus indicating that NO_2 reacts at least with the $MgCl_2$ hydrate and that the presence of hydrates may be of great importance in the reaction. De Haan and Finlayson-Pitts,[17] using a Knudsen cell and mass spectroscopy, found that the reaction of HNO_3 proceeded as readily on $MgCl_2 \cdot 6H_2O$ as on synthetic sea salt.

As shown in Figure 8, at 27 ± 4% RH, χ is ~80% after 11 s exposure to 3 mbar of NO_2. Thus, complete conversion of Cl^- to NO_3^- can be expected in on the order of 20 s at this NO_2 pressure. Figures 7 and 8 show that the conversion depends on both the NO_2 pressure and on the humidity. While the limited number of data points and the scatter in the data restrict the precision and accuracy of the kinetic data which may be obtained, it is nevertheless a valuable illustration of the utility of IR spectroscopy of aerosols. For the reaction of sea salt aerosol with NO_2, there is no evidence of a slow-down in the reaction even at $\chi = 80\%$. For a surface reaction, the rate should decrease as the surface is depleted of the reactant, unless there is some mechanism to rejuvenate the surface. Allen et al.[14] and Laux et al.[16] found that thin uniform layers of $NaNO_3$ formed on the surfaces of NaCl crystals would reorganize upon exposure to very low humidity to form $NaNO_3$ islands on a rejuvenated NaCl surface. A similar process might occur on the surfaces of the sea salt particles. If the particles exist as supersaturated solution droplets, then the reaction would be limited by the diffusion of the reactants in the solution, and thus the reaction may not slow appreciably even as χ approaches 100%.

Conclusion

We have reported here what appears to be the first in situ spectroscopic study of the reaction of NO_2 with sea salt aerosol. Although considerable uncertainties about the mechanism and the overall reaction remain, there is substantial conversion of Cl^- to NO_3^- in the sea salt particles. Moreover, the prominence of ClNO among the products points to $2NO_2 + Cl^- \rightarrow NO_3^- + ClNO$ as the dominant reaction pathway. The rate of the formation of nitrate depends both on the relative humidity and the pressure of nitrogen dioxide. The IR spectroscopic signatures for NO_3^- and H_2O indicate that the sea salt particles have a

complex internally mixed structure incorporating both liquid water and hydrated salts in both microcrystalline and amorphous phases. The spectra also reveal that even under arid conditions, sea salt aerosol retains a significant fraction of water and that the water content can increase as the reaction progresses. These results underscore the need to choose an appropriate substrate when studying heterogeneous chemistry. While supported powders of sea salt (or even NaCl) are experimentally convenient, these materials cannot retain the amount of water that appears to be incorporated in atmospheric sea salt aerosol. Further studies of the composition and morphology of the sea salt aerosol, its deliquescence and efflorescence properties, and quantitation of the gas-phase species are required for a more thorough understanding of this and related reactions to emerge. The partial pressure of NO_2 used in this investigation is 3 to 4 orders of magnitude higher than that found in highly polluted tropospheric air,[25] so it is unlikely that reaction A will be significant in the troposphere. Nevertheless, the IR spectra of the sea salt aerosols reveal that the particles possess a complex and dynamic structure that needs to be taken into account in laboratory studies and models of heterogeneous reactions.

Acknowledgment. The authors wish to thank the National Science Foundation for funding this research under Grant ATM96-31838. In addition, D.D.W. thanks the Pharmacia & Upjohn and Eli Lilly Companies for supporting fellowships.

References and Notes

(1) Warneck, P. *Chemistry of the Natural Atmosphere*; Academic Press: New York, 1988.
(2) Robbins, R. C.; Cadle, R. D.; Eckhardt, D. L. *J. Meterol.* **1959**, *16*, 53.
(3) Schroeder, W. H.; Urone, P. *Environ. Sci. Technol.* **1974**, *8*, 756.
(4) Finlayson-Pitts, B. J. *Nature* **1983**, *306*, 676.
(5) Winkler, T.; Goschnick, J.; Ache, H. J. *J. Aerosol Sci.* **1991**, *22*, S605.
(6) Junkermann, W.; Ibusuki, T. *Atmos. Environ.* **1992**, *26A*, 3099.
(7) Vogt, R.; Finlayson-Pitts, B. J. *J. Phys. Chem.* **1994**, *98*, 3747.
(8) Karlsson, R.; Ljungström, E. *J. Aerosol Sci.* **1995**, *26*, 39.
(9) Wan, J. K. S.; Pitts, J. N., Jr.; Beichert, P.; Finlayson-Pitts, B. J. *Atmos. Environ.* **1996**, *30*, 3109.
(10) Peters, S. J.; Ewing, G. E. *J. Phys. Chem.* **1996**, *100*, 14093.
(11) Langer, S.; Pemberton, R. S.; Finlayson-Pitts, B. J. *J. Phys. Chem. A* **1997**, *101*, 1277.
(12) Fenter, F. F.; Caloz, F.; Rossi, M. *J. Phys. Chem.* **1994**, *98*, 9801.
(13) Leu, M.-T.; Timonen, R. S.; Keyser, L. F. *J. Phys. Chem.* **1995**, *99*, 13203.
(14) Allen, H. C.; Laux, J. M.; Vogt, R.; Finlayson-Pitts, B. J.; Hemminger, J. C. *J. Phys. Chem.* **1996**, *100*, 6371.
(15) Beichert, P.; Finlayson-Pitts, B. J. *J. Phys. Chem.* **1996**, *100*, 15218.
(16) Laux, J. M.; Fister, T. F.; Finlayson-Pitts, B. J.; Hemminger, J. C. *J. Phys. Chem.* **1996**, *100*, 19891.
(17) De Haan, D. O.; Finlayson-Pitts, B. J. *J. Phys. Chem. A* **1997**, *101*, 9993.
(18) ten Brink, H. M. *J. Aerosol Sci.* **1998**, *29*, 57.
(19) Davies, J. A.; Cox, R. A. *J. Phys. Chem. A* **1998**, *102*, 7631.
(20) Timonen, R. S.; Chu, L. T.; Leu, M.-T.; Keyser, L. F. *J. Phys. Chem.* **1994**, *98*, 9509.
(21) Caloz, F.; Fenter, F. F.; Rossi, M. J. *J. Phys. Chem.* **1996**, *100*, 7494.
(22) Livingston, F. E.; Finlayson-Pitts, B. J. *Geophys. Res. Lett.* **1991**, *18*, 17.
(23) Behnke, W.; Scheer, V.; Zetzsch, C. *J. Aerosol Sci.* **1994**, *25*, S277.
(24) Fenter, F. F.; Caloz, F.; Rossi, M. J. *J. Phys. Chem.* **1996**, *100*, 1008.
(25) Wayne, R. P. *Chemistry of Atmospheres*, 2nd ed.; Oxford Science: Oxford, 1991.
(26) Finlayson-Pitts, B. J.; Pitts, J. N., Jr. *Atmospheric Chemistry: Fundamentals and Experimental Techniques*; Wiley: New York, 1986.
(27) Weis, D. D.; Ewing, G. E. *J. Geophys. Res.* **1999**. Manuscript accepted for publication.
(28) Cziczo, D. J.; Nowak, J. B.; Hu, J. H.; Abbatt, J. P. D. *J. Geophys. Res.* **1997**, *102*, 18843.
(29) Hinds, W. C. *Aerosol Technology: Properties, Behavior, and Measurement of Airborne Particles*; Wiley-Interscience: New York, 1982.
(30) *Handbook of Chemistry and Physics*, 79th ed.; Linde, D. R., Ed.; CRC Press: Boca Raton, 1998.
(31) Weis, D. D.; Ewing, G. E. *Anal. Chem.* **1998**, *70*, 3175.
(32) Weis, D. D.; Ewing, G. E. *J. Geophys. Res.* **1996**, *101*, 18709.
(33) Weis, D. D.; Ewing, G. E. *Glas. Hem. Technol. Maked* **1997**, *16*, 3.
(34) Bohren, C. F.; Huffman, D. R. *Absorption and Scattering of Light by Small Particles*; Wiley-Interscience: New York, 1983.
(35) Palik, E. D.; Khanna, R. Sodium Nitrate ($NaNO_3$). In *Handbook of Optical Constants*; Palik, E. D., Ed.; Academic Press: New York, 1998; Vol. 3, p 871.
(36) Sporleder, D. Personal communication.
(37) Weis, D. Infrared spectroscopy of aerosols: theory, techniques, and applications. Ph.D. Dissertation, Indiana University, 1998.
(38) Downing, H. E.; Williams, D. *J. Geophys. Res.* **1975**, *80*, 1656.
(39) Peters, S. J.; Ewing, G. E. *J. Phys. Chem. B* **1997**, *101*, 10880.
(40) Peters, S. J.; Ewing, G. E. *Langmuir* **1997**, *13*, 6345.
(41) Prentice, K. M. Infrared spectroscopic investigation of liquid water and ice aerosols. M.S. Thesis, Indiana University, 1997.
(42) Ewing, G. E.; Peters, S. J. *Surf. Rev. Lett.* **1997**, *4*, 757.
(43) Herzberg, G. *Infrared and Raman Spectra of Polyatomic Molecules*; Van Norstrand Reinhold: New York, 1945.
(44) Toon, O. B.; Pollack, J. B.; Khare, B. N. *J. Geophys. Res.* **1976**, *81*, 5733.
(45) Han, J.-H.; Martin, S. T. *J. Geophys. Res.* **1999**, *104*, 3543.
(46) *Dictionary of Inorganic Compounds*; Macintyre, J. E., Ed.; Chapmann and Hall: New York, 1992; Vol. 3.
(47) Mélen, F.; Herman, M. *J. Phys. Chem. Ref. Data* **1992**, *21*, 1992.
(48) Querry, M. R.; Waring, R. C.; Holland, W. E.; Hale, G. M.; Nijm, W. *J. Opt. Soc. Am.* **1972**, *62*, 849.
(49) Kester, D. R.; Duedall, I. W.; Connors, D. N.; Pytkowicz, R. M. *Limnol. Oceanogr.* **1967**, *12*, 176.
(50) Tang, I. N.; Tridico, A. C.; Fung, K. H. *J. Geophys. Res.* **1997**, *102*, 23269.
(51) Kato, R.; Rolfe, J. *J. Chem. Phys.* **1967**, *47*, 1901.
(52) Irish, D. E.; Walrafen, G. E. *J. Chem. Phys.* **1967**, *46*, 378.
(53) Irish, D. E.; Davis, A. R. *Can. J. Chem.* **1968**, *46*, 943.
(54) Wyckoff, R. W. G. *Phys. Rev.* **1920**, *16*, 149.
(55) Fuchs, R.; Kliewer, K.; Pardee, W. J. *Phys. Rev.* **1966**, *50*, 589.
(56) Fox, D.; Hexter, R. M. *J. Chem. Phys.* **1964**, *41*, 1125.
(57) Devlin, J. P.; Pollard, P.; Frech, R. *J. Phys. Chem.* **1970**, *53*, 4147.
(58) Tang, I. N.; Fung, K. H. *J. Chem. Phys.* **1997**, *106*, 1653.
(59) Cheng, R. J. The generation of secondary marine aerosols: The crystallization of seawater droplets. In *Atmospheric Aerosols and Nucleation*; Wagner, P. E., Vali, G., Eds.; Springer-Verlag: New York, 1988; p 589.
(60) Cheng, R. J.; Blanchard, D. C.; Cipriano, R. J. *Atmos. Res.* **1988**, *22*, 15.
(61) Mowaka, E. J. Personal communication.
(62) Arakawa, E. T.; Nielsen, A. H. *J. Mol. Spectrosc.* **1958**, *2*, 413.
(63) Burns, W. G.; Bernstein, H. J. *J. Chem. Phys.* **1950**, *18*, 1669.
(64) Bibart, C. H.; Ewing, G. E. *J. Chem. Phys.* **1974**, *61*, 1284.
(65) Keller, F. L.; Nielsen, A. H. *J. Chem. Phys.* **1956**, *24*, 636.
(66) IUPAC *Tables of Wavenumbers for the Calibration of Infra-Red Spectrometers*; Butterworth: Washington, DC, 1961.
(67) Landau, L.; Fletcher, W. H. *J. Mol. Spectrosc.* **1960**, *4*, 276.
(68) McGraw, G. E.; Bernitt, D. L.; Hisatsune, I. C. *J. Chem. Phys.* **1965**, *42*, 237.
(69) McGraw, G. E.; Bernitt, D. L.; Hisatsune, I. C. *J. Chem. Phys.* **1966**, *45*, 1392.